

**Supporting Information for**  
**Self-assembled Nanoscale DNA-porphyrin Complex for**  
**Artificial Light-harvesting**

*Jakob G. Woller, Jonas K. Hannestad, and Bo Albinsson*

Department of Chemical and Biological Engineering/Physical Chemistry, Chalmers  
University of Technology, S-41296 Gothenburg, Sweden

**Contents**

Light harvesting properties of the pseudo-hexagonal complex	S2
Antenna effect calculation	S3
Theoretical model of multi-step energy transfer based on homo-transfer	S4
The Markov chain model	S4
Simulation	S7
Energy transfer distance distribution	S10
YO-PRO-1 fluorescence anisotropy	S12
Formation of Pseudo-hexagon structures	S15
References	S16

## Light harvesting properties of the pseudo-hexagonal complex

Excitation spectra at varying YO:bp mixing ratios for the 99 bp pseudo-hexagonal complex are presented in figure S1. The YO:bp binding ratio is used as opposed to YO:porphyrin ratio, which was used in the main text, to ease in comparisons of the two systems. The spectra at the ratios 0.25 (~25 YO:porphyrin), 0.5, and 1 have been corrected for differing concentrations of construct, due to dilution (see main text). An increase in the antenna effect was seen when going from the mixing ratio 0.5 to 1 indicating that an excess of YO was needed to saturate the DNA with intercalators. Effective absorption coefficient ( $\epsilon_{eff}$ ), antenna effect ( $AE$ ) and overall transfer efficiency ( $E$ ) data are presented in table S1. Antenna effects and effective absorption coefficients were calculated as described below and in the main text, equation 4.

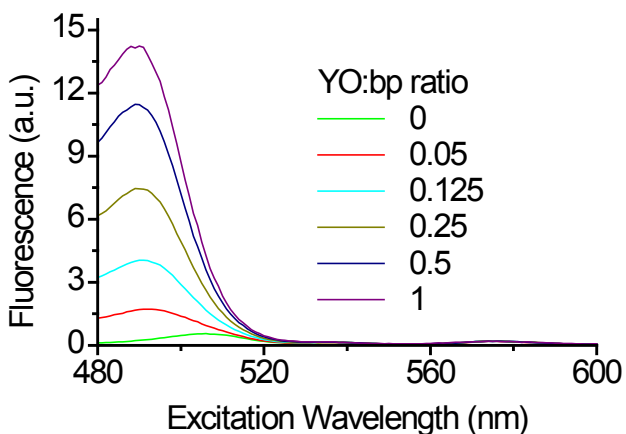


**Figure S1** Fluorescence excitation spectra monitored at the porphyrin emission peak at 700 nm as a function of increasing YO:bp mixing ratio for the pseudo-hexagonal construct.

**Table S1. Light harvesting properties of the pseudo-hexagon DNA complex at varying YO:bp ratios.**

YO:bp ratio	$E^a$	$AE^b$	$\epsilon_{eff} (10^3 \cdot M^{-1} cm^{-1})^c$
0.05	0.26±0.003	1.7	37
0.125	0.22±0.003	4.6	100
0.25	0.20±0.01	8.8	190
0.5	0.18±0.005	14	310
1	0.21	17	370

<sup>a</sup>Overall transfer efficiency. Standard deviations based on two measurements are shown where available. <sup>b</sup>Antenna effect. <sup>c</sup>Effective absorption coefficient.

### Antenna effect calculation

The antenna effect was calculated from excitation spectra using equation S1. All fluorescence spectra were corrected for lamp intensity.

$$AE = \frac{I_{DA,491} \cdot f_{I_A} - I_{A,491}}{I_{A,505}} \quad (S1)$$

where  $I_{DA,491}$  is the fluorescence at 700 nm when exciting the donor-acceptor complex at 491 nm,  $f_{I_A}$  is the fraction of the total fluorescence at 700 nm stemming from the acceptor (this value was calculated from normalized fluorescence emission spectra, see figure S2, and varied between 0.95 for the wire construct to 0.65 for the pseudo-hexagon),  $I_{A,491}$  is the fluorescence at 700 nm of the acceptor only complex (porphyrin and DNA, no YO) when exciting at 491 nm,  $I_{A,505}$  is the fluorescence at 700 nm when exciting the acceptor only complex at its peak at 505 nm.

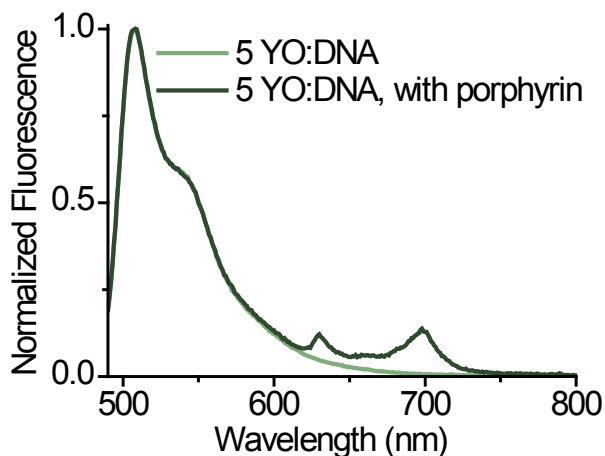


**Figure S2** Normalized fluorescence spectra of donor alone (YO intercalated in 39 mer DNA wire) and donor-acceptor (YO intercalated in porphyrin-modified DNA wire) complexes at 5 YO:DNA strand mixing ratio. At 700 nm (the emission wavelength for excitation spectra in main text) the porphyrin fluorescence contributes 95 % of the signal. Excitation wavelength was 483 nm.

## **Theoretical model of multi-step energy transfer based on homo-transfer**

### **The Markov chain model**

This model has been used to simulate fluorescence depolarization in DNA based multi-chromophoric systems capable of homo-transfer. A detailed description of the model is given by Carlsson *et al* where it is used to describe fluorescence depolarization of intercalated YO.<sup>1</sup> Here we present a basic outline with our modifications to the main model. The model is based on a series of individual transfer rates describing energy transfer from a single chromophore to any of the other chromophores in the system. The energy transfer rate constant between donor and acceptor,  $k_{EET}$ , is described by

$$k_{EET} = \frac{1}{\tau_D} \frac{3}{2} \kappa^2 \left( \frac{R_0}{R} \right)^6 \quad (\text{S2})$$

where  $R$  is the inter-chromophore distance,  $\tau_D$  the decay time of the donor in the absence of the acceptor,  $\kappa^2$  an orientation factor spanning from 0 to 4 and which is 2/3 for freely rotating chromophores, and  $R_0$  is the dynamically averaged Förster radius for the FRET pair, defined in the main text, equation 2.  $R_0^{\text{DA}}$  is used to calculate the rate constant for energy transfer to the acceptor (porphyrin) and  $R_0^{\text{DD}}$  is used to calculate energy transfer from a donor to another donor (YO to YO, homo-FRET).

The  $R_0$ -values ( $R_0^{\text{DA}}$  and  $R_0^{\text{DD}}$ ) are determined assuming freely rotating chromophores and the term  $3\kappa^2/2$  in equation S2 is used as a correction factor where this is not the case, *i.e.* for energy transfer between any two YO molecules, where the orientation is taken into account directly from the structure of B-DNA and unwinding of the DNA helix. For excitation energy positioned on a given chromophore the probabilities to jump to chromophore  $j$  in one step or to leave the system are, respectively,

$$p_{ij} = \frac{k_{ij}}{k_i + \sum_{i \neq l} k_{il}} \quad (\text{S3})$$

$$p_{i,\text{out}} = \frac{k_i}{k_i + \sum_{i \neq l} k_{il}} \quad (\text{S4})$$

Here  $k_{ij}$  is the transfer rate given by equation S2,  $k_i$  is the sum of the radiative and non-radiative decay rates of chromophore  $i$  ( $k_i = 1/\tau_i$ ) and the summations in equation S3 and S4 are over all energy transfer rates from chromophore  $i$ .

For a DNA system with  $N$  intercalating chromophores at saturation and one covalently attached chromophore there are  $N+1$  different chromophore positions. The distribution of excitation energy after a discrete number of steps (transfers)  $n$  is described by a row matrix,  $\mathbf{v}_n$  (equation S5). The first  $N+1$  rows describe the initial distribution of excitation energy on the various chromophores. The last  $N+1$  rows describe the distribution of excitation energy after  $n$  steps. By combining the initial distribution of excitation energies,  $\mathbf{v}_0$  (where the last  $N+1$  rows are zero) with a matrix ( $\mathbf{M}$ ) consisting of the energy transfer and emission probabilities described above, the energy distribution after an arbitrary number of steps can be described.

$$\mathbf{v}_n = \mathbf{v}_{n-1} \cdot \mathbf{M} = \dots = \mathbf{v}_0 \cdot \mathbf{M}^n \quad (\text{S5})$$

The matrix  $\mathbf{M}$  can be divided into four  $(N+1) \times (N+1)$  submatrices

$$\mathbf{M} = \begin{pmatrix} \mathbf{A} & \mathbf{D} \\ \mathbf{0} & \mathbf{I} \end{pmatrix} \quad (\text{S6})$$

where  $\mathbf{0}$  and  $\mathbf{I}$  are the zero and unity matrices, respectively,  $\mathbf{A}$  has a zero diagonal with the other elements equal to  $p_{ij}$ , and  $\mathbf{D}$  is a diagonal matrix containing  $p_{i,out}$  as diagonal elements.

The limit of the matrix  $\mathbf{M}$  to the power of  $n$  when  $n$  goes to infinity is

$$\lim_{n \rightarrow \infty} \mathbf{M}^n = \begin{pmatrix} \mathbf{0} & (\mathbf{I} - \mathbf{A})^{-1} \mathbf{D} \\ \mathbf{0} & \mathbf{I} \end{pmatrix} \quad (\text{S7})$$

The steady state distribution of energy is described by the limiting value after an infinite number of steps:

$$\mathbf{v}_\infty = \mathbf{v}_0 \cdot \lim_{n \rightarrow \infty} \mathbf{M}^n \quad (\text{S8})$$

By monitoring the  $\mathbf{v}_\infty$  row matrix for different DNA constructs the probability of the excitation energy leaving the system for each chromophore can be determined.

## Simulation

Simulation of energy transfer in the DNA light harvesting complexes containing YO and porphyrin was performed according to the model described above. In each multichromophoric system there are  $N+1$  chromophore positions, with  $N$  being the maximum number of intercalators. Each position is associated with a coordinate along the DNA strand depending on the position of the chromophore. The first possible intercalation position was used as a reference point and positioned at the origin in the

coordinate system. The positions of all the other chromophores were expressed by their distance to this YO position. The intercalating YO molecules were positioned randomly in the DNA sequence obeying nearest neighbor exclusion. Every intercalation results in an extension of the strand of one base pair (3.4 Å). For the 39-mer wire construct, the porphyrin was positioned 19 bases from the origin along the DNA strand (taking into account strand extension by intercalated YO), and 24 Å away from the DNA (a distance corresponding to the linker length, see cartoon in figure 1B in the main text). The distance along the DNA from the origin to where the linker between porphyrin and DNA meets the DNA is one cathetus in a right-angled triangle, where the other cathetus is given by the linker length. The distance from the origin to the porphyrin is then the hypotenuse of this triangle. The porphyrin was assigned as the first element in all matrices.

A number of experimental parameters were used in the simulation. In order to calculate the transfer rates given by equation S2, the donor lifetime and quantum yield are needed. For YO both these parameters vary with the ratio of YO:bp (YO molecules to DNA base-pairs),  $r$ . Fluorescence quantum yields and lifetimes of YO were determined as a function of  $r$  (figure S3). The intensity-weighted average fluorescence lifetimes of YO,  $\tau_D$ , as a function of intercalator density were fitted using an exponential function yielding  $\tau_D = 1.17 \exp(-r/0.2) + 2.2$ . The Förster distances of the involved donor-acceptor pairs were calculated using a variable quantum yield for YO. Applying an exponential fit also to the fluorescence quantum yield data yielded the following relationship between YO fluorescence quantum yield and intercalator density;  $QY_D = 0.35 \exp(-r/0.26) +$

0.13. For YO to YO homo-FRET the variation in  $QY_D$  results in  $R_0^{DA}$  values ranging from 43 Å at low YO density to 32 Å at YO saturation. The changes in  $QY_D$  and  $\tau_D$  reflect both an increase in non-radiative decay, yet also a decrease in the rate constant of fluorescence,  $k_f$  (figure S3D). This decrease is likely due to excitonic coupling between YO molecules in close proximity. At high mixing ratios above 0.2 another possibility is that binding modes other than intercalation play a role, as has previously been observed.<sup>2</sup> This may contribute to the changes observed here, since other binding modes are likely to yield different radiative and non-radiative rate constants.

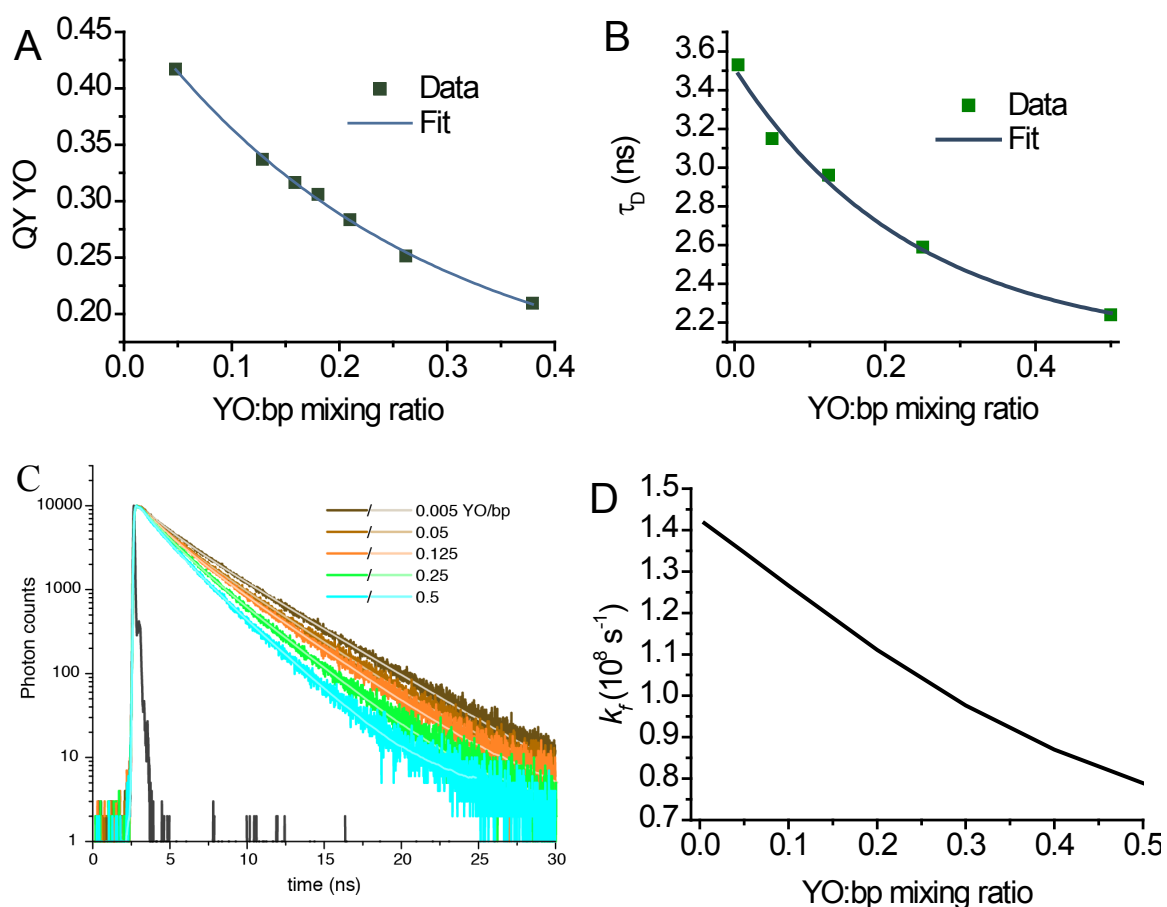


**Figure S3 A)** Fluorescence quantum yield of YO intercalated in DNA as a function of YO:bp density. An exponential fit to the data is shown, which was used in the simulation.

**B)** Intensity-weighted average lifetime of YO intercalated in DNA as a function of

YO:bp density. An exponential fit to the data is shown, which was used in the simulation. **C)** Time correlated single photon counting histograms at varying YO:DNA ratio. Deconvoluted bi-exponential fits are shown for each binding ratio. **D)** The fluorescence rate constant,  $k_f = QY_D/\tau_D$ , of YO as a function of YO:bp mixing ratio.

The simulation was initiated by forming the  $\mathbf{v}_0$  row matrix giving the initial distribution of excitation energy. Here, an approximation was made assuming exclusive excitation of YO. A random YO is excited resulting in a  $\mathbf{v}_0$  with the first element equal to zero (the porphyrin element), a random element assigned the value one, with zeros in all other elements. The output was monitored by following the  $N+2$  term in the  $\mathbf{v}_\infty$  row matrix, representing the fraction of initial excitation energy reaching the acceptor.

Simulations were performed up to 10,000 times for each single YO binding density between 0.005 and 0.5 and the average porphyrin emission value was recorded. To compensate for the dynamics in the binding of YO to DNA a Poisson distribution of intercalated YO molecules around the selected average ( $N$ ) was used.

The simulation assumes that YO only binds to DNA through intercalation. However, at high YO/base pair ratios (above 0.2) there is a significant fraction of YO molecules that bind to DNA in other ways than through intercalation.<sup>2</sup>

To simulate the DNA pseudo-hexagon structure some simplifications were made compared to the wire structure. Due to the flexibility of the hexagon the orientation factor

$\kappa^2$  was set to 2/3 (random orientation of the fluorophores). Similarly, the extension of the DNA structure by 3.4 Å for each intercalator was not included in the simulations of the pseudo-hexagon structure. Also, the porphyrin was positioned 30 bp from the end of the arm of the pseudo hexagon (see figure 7 in the main text).

### **Energy transfer distance distribution**

The fluorescence decay curves of the DNA-porphyrin samples at varying YO concentration were fitted using the Lorentzian distribution described in the main text (equations 5 and 6). Using a distribution function instead of a sum of exponentials to describe the fluorescence decay can yield physically relevant qualitative information about the system which otherwise would not be obtained. Using a sum of exponentials would undoubtedly yield better fits to the data, yet would not be a physically relevant description of the system. It is important to clarify that the choice of distribution function is arbitrary, and the Lorentzian distribution was chosen as a likely possible candidate since it can describe the expected apparent distribution of donor positions, as the concentration of donors increases. The fitting routine was implemented in MatLab 7. The reduced  $\chi^2$  value and inspection of the residuals were used to determine how well data fitted to the model. Figure S4A and S4B show the fitted decays for the assemblies with long and short linkers, respectively.

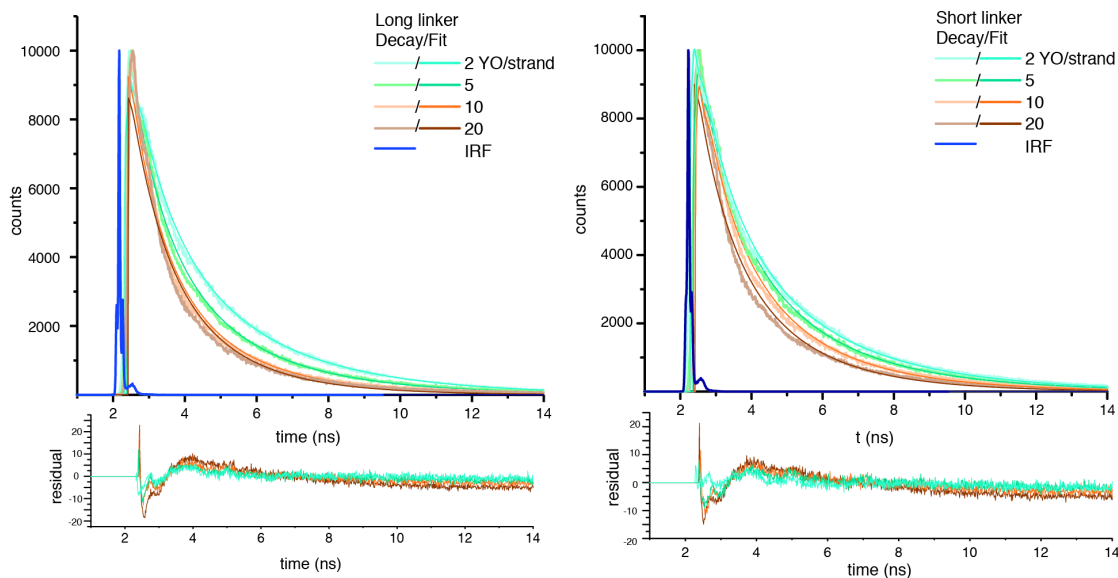


**Figure S4** Fluorescence intensity decays for YO-PRO-1 intercalated in DNA-Porphyrin assemblies. The decay curves represent the systems with **A)** long and **B)** short linkers at different intercalator concentrations. The decay curves are fitted to a Lorentzian distribution function according to equations 5 and 6 in the main text.

### **YO-PRO-1 fluorescence anisotropy**

The fluorescence anisotropy describes the depolarization of emission following excitation using polarized light. In the case of YO-PRO-1 bound to 39-mer DNA (a cylindrical rod) the two axes of rotation can in principle give rise to anisotropy decay. The two rotations occur around the long and short axes. Rotation around the long axis (the axis of symmetry) is rapid and on the time-scale of the fluorescence lifetime. Rotation around the short axis is much slower, and therefore does not contribute to the observed anisotropy decay. The anisotropy decay is therefore approximately described by a function which decays mono-exponentially with time (equation S9)

$$r(t) = r_0 e^{-t/\theta} \quad (\text{S9})$$

where  $r$  is the anisotropy,  $r_0$  the anisotropy at  $t=0$  and  $\theta$  the rotational correlation time. When the concentration of YO-PRO-1 increases, homo-FRET causes a depolarization of the YO emission, yielding a more rapid anisotropy decay. To obtain the fluorescence anisotropy the fluorescence decay from YO-PRO-1 bound to DNA was recorded at both vertical (V) and horizontal (H) polarization, each using both horizontally and vertically polarized excitation yielding four different recorded signals ( $I_{VV}$ ,  $I_{VH}$ ,  $I_{HV}$  and  $I_{HH}$ ). The anisotropy is given by equation S10<sup>3</sup>

$$r = \frac{I_{VV} - GI_{VH}}{I_{VV} + 2GI_{VH}} \quad (\text{S10})$$

where  $G$  is a correction for anisotropy in the detection efficiency and is given by equation S11

$$G = \frac{I_{HV}}{I_{HH}} \quad (\text{S11})$$

Samples were excited using a pulsed laser diode emitting at 483 nm (PicoQuant) with 10 MHz repetition rate and ~100 ps pulse-width (fwhm). Emission was recorded at 510 nm and the emitted photons were collected by a thermoelectrically cooled micro-channel plate photomultiplier tube (R3809U-50, Hamamatsu). The signal was digitalized using a

multichannel analyzer with 4096 channels (SPC-300, Edinburgh Analytical Instruments). A global analysis of the polarized fluorescence intensity decay curves of samples containing only DNA and YO-PRO-1 was performed to directly obtain  $r$ , using the program FluoFit Pro v.4 (PicoQuant GmbH). The global parameters were two lifetimes and amplitudes for the YO-PRO-1 fluorescence decay and a single rotational correlation time and limiting anisotropy  $r_0$ . Figure S5A shows the resulting fitted anisotropy decay curves at varying YO:porphyrin mixing ratios. Figure S5B shows correlation times obtained from the fitted data shown in figure S5A, including an exponential fit to the data. Rotational correlation times based on the time-resolved anisotropy decays for YO intercalated in DNA are collected in table S2.

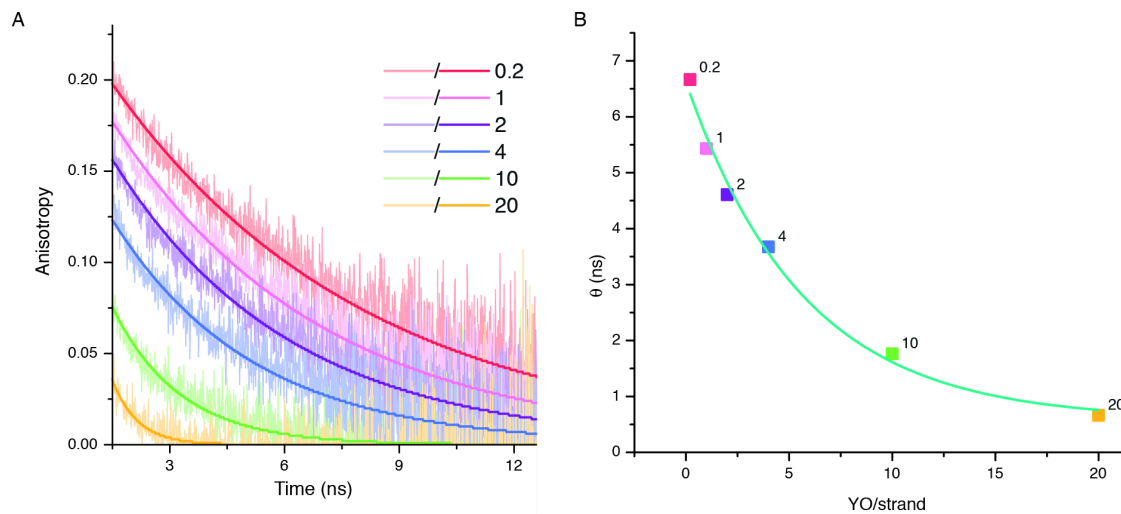


**Figure S5 A)** Anisotropy decay of YO intercalated in DNA at different YO/strand ratios. Note the differences in  $r_0$  indicating that some of the anisotropy decay is not fully resolved. **B)** Exponential fit of correlation time as function of intercalator density (YO/strand).

**Table S2 Rotational correlation time ( $\theta$ ), anisotropy at time zero ( $r_0$ , pre-exponential factor in equation S9), and reduced chi-square values as a function of intercalator density**

YO/strand	$\theta$ (ns)	$r_0$	$\chi^2$
<b>0.2</b>	6.67	0.20	1.19
<b>1</b>	5.43	0.19	1.07
<b>2</b>	4.61	0.17	1.07
<b>4</b>	3.67	0.12	1.16
<b>10</b>	1.76	0.08	1.08
<b>20</b>	0.66	0.05	1.03

### Formation of Hexagon structures

The sequences used to form the pseudo-hexagon structures were chosen based on previous work, and are shown in table S3 and figure S6.<sup>4,5</sup>

**Table S3. DNA strands used for hexagon structure formation**

Strand nr.	Sequence
<b>1</b>	<b>CGTCTGAGTGTGTCTAGCTGATTGGTTGGGATTGCGGCCTT GACGCTAATCTTGATGCTGTGG</b>
<b>2</b>	<b>GATTAGCGTCTTCGATGGTATC</b>
<b>3</b>	<b>GGCTCTACAGTTGAGGAGGATG</b>
<b>4</b>	<b>CTGTAGAGCCTTGATACCATCG</b>
<b>5</b>	<b>CCATACATACTTCCACAGCATC</b>
<b>6</b>	<b>GTATGTATGGTTCATCCTCCTC</b>
<b>7</b>	<b>GGCCGCAAT<sup>T<sup>porphyrin</sup></sup>CCCAACCAATCAGCTAGACACACTCAGA CG</b>
<b>8</b>	<b>GGCCGCAATCCCAACCAATCAGCTAGACACACTCAGACG</b>

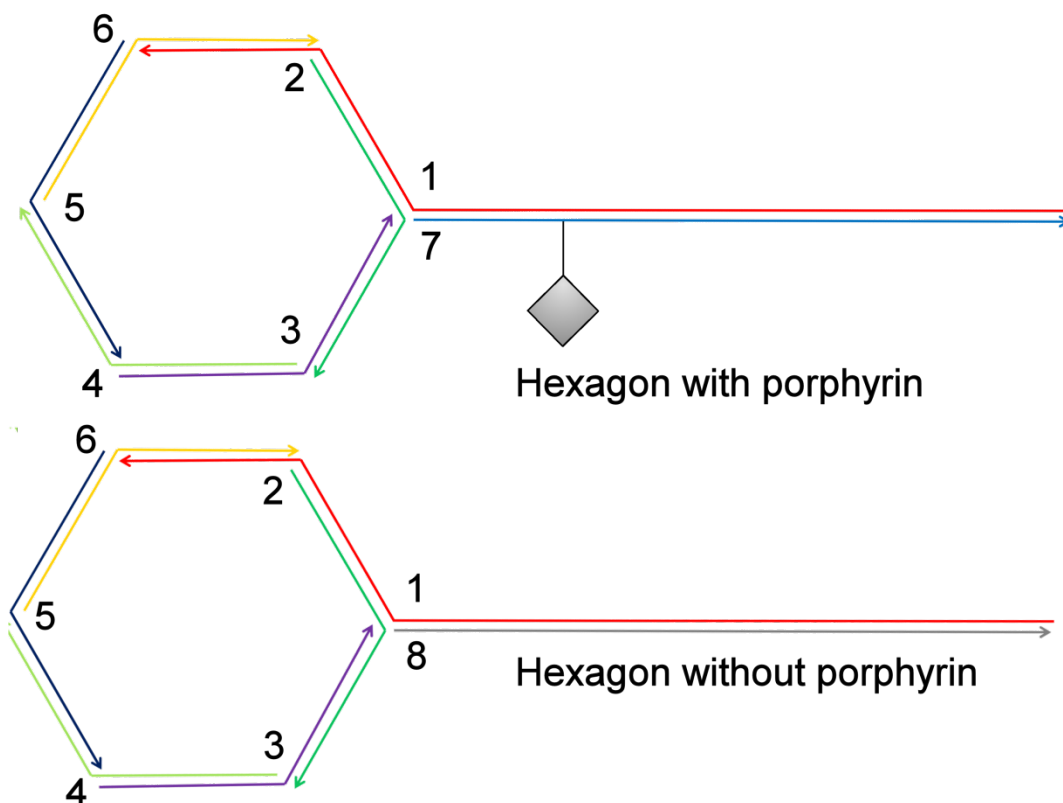


**Figure S6** Schematic diagram of the two pseudo-hexagonal DNA structures used. The strands are color coded and numbered according to table S3.

## References

1. Carlsson, C. L., A.; Björkman, M.; Jonsson, M.; Albinsson, B. *Biopolymers* **1997**, *41*, 481-494.
2. Larsson, A.; Carlsson, C.; Jonsson, M.; Albinsson, B. *J. Am. Chem. Soc.* **1994**, *116*, 8459-8465.
3. Lakowicz, J. R., *Principles of Fluorescence Spectroscopy*. 3 ed.; Springer: New York, 2006.
4. Börjesson, K.; Lundberg, E. P.; Woller, J. G.; Nordén, B.; Albinsson, B. *Angew. Chem. Int. Ed.* **2011**, *50*, 8312-8315.
5. Tumpene, J.; Sandin, P.; Kumar, R.; Powers, V. E. C.; Lundberg, E. P.; Gale, N.; Baglioni, P.; Lehn, J. M.; Albinsson, B.; Lincoln, P.; Wilhelmsson, L. M.; Brown, T.; Nordén, B. *Chem. Phys. Lett.* **2007**, *440*, 125-129.